Size-dependent properties of functional PPV-based conjugated polymer nanoparticles for bioimaging

Peer-reviewed author version

Size-Dependent Properties of Functional PPV-based Conjugated Polymer Nanoparticles for Bioimaging.

Martijn Peters[a], Senne Seneca[a], Niels Hellings[c], Tanja Junkers[a,b], Anitha Ethirajan[a,b]*.

[a] Institute for Materials Research, Hasselt University, Martelarenlaan 42, 3500 Hasselt, Belgium.

[b] Imec associated lab IMOMEC, Wetenschapspark 1, 3590 Diepenbeek, Belgium.

[c] Immunology-Biochemistry, Biomedical Research Institute, Hasselt University, Agoralaan Building C, 3590 Diepenbeek, Belgium.

Corresponding Author Details:

E-mail: anitha.ethirajan@uhasselt.be

Phone number: +32-11268877

ABSTRACT

Conjugated polymer nanoparticle systems have gained significant momentum in the bioimaging field on account of their biocompatibility and outstanding spectroscopic properties. Recently, new control procedures have spawned custom-built functional poly(p-phenylene vinylene) (PPV). These facilitate the one-pot synthesis of semiconducting polymer NPs with incorporated surface functional groups, an essential feature for advanced biomedical applications. In this work, nanoparticles (NPs) of different sizes are synthesized consisting of the statistical copolymer CPM-co-MDMO-PPV with monomer units 2-(5'-methoxycarbonylpentyloxy)-5-methoxy-1,4-phenylenevinylene (CPM-PPV) and poly(2-methoxy-5-(3',7'-dimethoxyoctyloxy)-1,4-phenylenevinylene) (MDMO-PPV). To monitor potential implications of switching from a commonly used homopolymer to copolymer system, MDMO-PPV NPs were prepared as a control. The versatile combination of the miniemulsion and solvent evaporation method allowed for an easy adaptation of the NP size. Decreasing the diameter of functional PPV-based NPs up to 20 nm did not significantly affect their optical properties nor the biocompatibility of the bioimaging probe, as cell viability never dropped below 90 %. The quantum yield and molar extinction coefficient remained stable at values of 1-2 % and 10^6 M$^{-1}\cdot$ cm^{-1} respectively, indicating an excellent fluorescence brightness. However, a threshold was observed to which the size could be lowered without causing irreversible changes to the system. Cell uptake varied drastically depended on size and material choice, as switching from homo- to copolymer system and lowering the size significantly increased NP uptake. These results clearly demonstrate that adjusting the size of functional PPV-based NPs can be achieved easily to a lower limit of 20 nm without adversely affecting their performance in bioimaging applications.

INTRODUCTION

Immense endeavors have been made during the last decades to visualize and gain a more thorough insight into the extensive array of biological activities in living systems on the molecular and cellular level.[1-4] Fluorescence imaging is a technique that allows researchers to bring about this ambition by providing a high temporal and spatial resolution in combination with an excellent signal-to-noise ratio. The adoption of conventional fluorescent visualization agents, including organic fluorophores as well as fluorescent nanoparticles (NPs) such as quantum dots and dye-doped silica colloids, have culminated in considerable advances in the biomedical field. Regardless of this impressive feature, each material system still has its own deficiencies and intrinsic restraints.[5-12] For instance, the long established low molecular weight organic dyes are often plagued by a poor photostability and rapid cellular efflux. These obstacles can be surmounted by encapsulating them in NPs or by shifting to other options like quantum dots and nanodiamond. Nevertheless, these systems face other obstacles. NPs with encapsulated dyes often encounter pigment leakage or self-quenching and the use of quantum dots is still under debate given their short- and long-term cytotoxicity issues as well as *in vivo* degradation. Albeit nanodiamonds solve most of the aforementioned problems, dispersing them into single nanoparticles without causing contamination is a demanding task.[13]

Due to the remaining shortcomings of the preceding material classes, water-based colloidal dispersions consisting of fluorescent conjugated polymers have gained great acclaim within the bioimaging field.[14-21] The reason for this is their ultra-bright photoluminescence, owing to their π-conjugated backbone, in conjunction with an excellent biocompatibility. A prominent example amongst semiconducting polymers is poly(*p*-phenylenevinylene) (PPV), which is mostly known for being the pioneer material in the first organic light emitting diode constructs and has since been exploited in a wide variety of applications like biological sensors, solar cells and various other optoelectronic devices. Its acclaim can be ascribed to its well-known photophysical properties and dependable synthesis routes, like the sulfinyl precursor route, that can be used to devise state-of-the-art custom-made functional PPVs while being simple to scale up.[22-26] These complex functionalized PPVs grant an easy and elegant way to generate NPs with functional groups distributed on the surface that

can be employed for the on demand attachment of various nature- or man-made entities.[20] This has tremendous potential in the biomedical field where there is a never-ending appeal for the incorporation of different functional properties (stealth effect, barrier crossing potential, etc.) to permit control over biological and chemical traits.

Alongside surface alteration, NP size is one of the most critical concerns for biomedical applications as it has been identified to play a key role in biological processes like cellular uptake, biodistribution and cytotoxicity.[27, 28] Effective internalization by cells is essential to achieve the successful application of NPs for bioimaging objectives. In addition, adjusting the size can have an influence on the optical properties of conjugated polymer NPs.[29] Here, we probe for the first time the potential consequences of lowering the size of functional PPV-based NPs on the optical and biological characteristics of a conjugated system specifically designed for bioimaging purposes. The NP's core material consists of the functional statistical copolymer with monomer units 2-(5'-methoxycarbonylpentyloxy)-5-methoxy-1,4-phenylenevinylene and poly(2-methoxy-5-(3',7'-dimethoxyoctyloxy)-1,4-phenylene-vinylene) (CPM-PPV-*co*-MDMO-PPV, for simplicity henceforth called CPM-*co*-MDMO-PPV). The ester groups available at the CPM-*co*-MDMO-PPV NPs surface are of particular significance as they can be conveniently converted into carboxylic acid groups, enabling facile coupling of various biomolecules on demand. Since most PPV-based NP studies only focus on homopolymers, MDMO-PPV NPs were included to demonstrate the potential consequences of transitioning from this system to a statistical copolymer type. Size adaptation was achieved by implementing subtle changes in the synthesis method, a combination of the miniemulsion and solvent evaporation method.[20, 21, 30] Subsequently, the effects of varying the size on the colloidal, optical and biological properties of the water-based bioimaging agent were studied in detail.

METHODS

Chemicals and reagents

Rhodamine 6G (dye content 99 %), penicillin/streptomycin (P/S), hydrocortisone (HC), L-glutamine, trypsine, paraformaldehyde (PFA), triton X-100 were purchased at Sigma-Aldrich (Diegem, Belgium). Human microvascular endothelial cells (HMEC)-1 (CRL-3243) were bought at ATCC (Molsheim, France). MCDB 131 medium, fetal calf serum (FCS), recombinant human epidermal growth factor (EGF), iscove's modified dulbecco's medium (IMDM) medium and alamar blue were obtained from Life Technologies (Ghent, Belgium). All culture and dark plates were bought at Greiner Bio One (Vilvoorde, Belgium). The 1x phosphate buffered saline (1xPBS) was purchased at Lonza (Verviers, Belgium). Sodium dodecyl sulfate (SDS) was bought at GE Healthcare Life Sciences (Diegem, Belgium). Spectrum™ Spectra/Por 3 Regenerated Cellulose Dialysis Membrane Tubing (3.5 kD, 45 mm flat width) were bought at Fisher Scientific (Merelbeke, Belgium). All chemicals were used as provided without further purification.

PPV-Based NPs of various sizes: synthesis procedure

The synthesis procedure of the conjugated polymer and NPs was performed as described elsewhere.[20] NPs consisting of either MDMO-PPV (Mn = 150 000 g·mol^{-1}) or the copolymer CPM-*co*-MDMO-PPV (Mn = 164 200 g·mol^{-1}, 66:34 MDMO:PPV ratio as determined by ^{1}H NMR) were constructed employing a combination of the miniemulsion and solvent evaporation method. In order to generate different sizes of NPs various amounts of polymer (50, 25, 10, 5 and 1 mg) were used in the synthesis procedure and the surfactant SDS used was 100 mg in 24 g of ultrapure water solution. The continuous phase, consisting of SDS and ultrapure water, and dispersed phase, consisting of the conjugated polymer in CHCl$_3$, are mixed together to pre-emulsify. This mixing step is followed by ultrasonication (1/4"-tip, 3 min, 65 % amplitude, 30 s pulse and 20 s pause regime) under ice cooling to generate nanodroplets of which the organic solvent is evaporated at 40°C overnight. This results in

a colored dispersion of PPV-based NPs in water after filtration (Whatman, pore size 4–7 μm) of the sample to remove any large aggregates present.

PPV-Based NPs of various sizes: washing, reconcentration and characterization

After synthesis, the NPs underwent 40 washing steps of 1 hour employing Spectrum™ Spectra/Por 3 Regenerated Cellulose Dialysis Membrane Tubing (3.5 kD, 45 mm flat width) at 500 rpm with ultrapure water. Subsequently, the samples were reconcentrated through evaporation at 40 °C with 500 rpm stirring. The reconcentrated NP samples were sterilized using an IBL 437C type gamma radiator (Cis Bio International, Codolet, France) at 30 Gy (= 3000 rad) after which they were stored in the dark.

The hydrodynamic diameter, polydispersity (PD) and zeta potential were determined using dynamic light scattering with Brookhaven Instrument Cooperation ZetaPALS equipment (Waddinxveen, The Netherlands). The PD value (ranging between 0-1) generated by the software is a measure for the particle size distribution. The lower the PDI values, narrower the size distribution. The zeta potential of nanoparticles was measured in 10^{-3} M KCl solution at 20°C. In parallel, the study of size and morphology of the NPs was performed with TEM at an accelerating voltage of 120 keV using a FEI Tecnai G2 spirit twin (Zaventem, Belgium), after drop casting and drying the respective samples on copper grids. TEM data are represented as means ± standard deviation after measuring 25 NPs per sample using ImageJ software, which was also used to process the images. As the solutions were dilute, the solid contents were obtained by determining the amount of conjugated polymer in a given volume from their measured absorbance using the Agilent Technologies Cary 5000 UV-VIS-NIR spectrophotometer (Diegem, Belgium). For this, a calibration curve of the absorbance of various conjugated polymer concentrations (10, 25, 50, 100, 250, 500, 1000, 2500 μg/mL) for MDMO-PPV and CPM-*co*-MDMO-PPV in CHCl$_3$ was constructed. The respective NP samples were dried and redissolved in CHCl$_3$ after which the absorbance was measured and used to calculate the solid content.

Influence of NP Size on Optical Characteristics of PPV-Based NPs

The optical spectrum of PPV-based NPs of different sizes and PPVs were measured in a 1 cm quartz cuvette with the Cary 5000 UV-VIS-NIR spectrophotometer and Horiba Jobin Yvon Fluorolog3 Tau fluorescence spectrophotometer (Lier, Belgium). The wavelength dependence of the throughput and sensitivity of the detection channel were corrected for the emission spectra.

A comparison was made between the different NP sizes for the molar extinction coefficient, absorption cross-section and quantum yield (QY). The Beer-Lambert Law was used to calculate the molar extinction coefficient of the NPs, by varying their concentration in water, and subsequently used to determine the absorption cross-section. The QY was determined with rhodamine 6G as fluorescence reference (QY = 0.95, in H_2O). Five dilutions were prepared for all samples and reference, the absorbance of the most concentrated one reaching a value of 0.1 at 490 nm excitation to which the standard was optically matched. For each of these sample dilutions the emission spectrum correlated to the respective excitation wavelength was measured and the absorption versus integral of emission spectrum was plotted. The obtained slope value (m) of the fitted trend line and refractive indexes (η) of the liquids were inserted into the following formula to obtain the QY.

$$QY_{SAMPLE} = QY_{STANDARD} \times \frac{m_{SAMPLE}}{m_{STANDARD}} \times \frac{\eta^2_{SAMPLE}}{\eta^2_{STANDARD}}$$

Subsequently, the fluorescence brightness of the NPs (B_{NP}) was determined through multiplication of the quantum yield and molar extinction coefficient.

Influence of NP size on Biological Characteristics of PPV-Based NPs

Cell Culture. The HMEC-1 cell line was maintained in a T25 flask in culture medium (MCDB 131 medium supplemented with 10 % FCS, 0.5 % P/S, 500 ng EGF, 50 µg HC, 500 µmol L-Glutamine) stored at 37 °C in a 5% CO_2 incubator (Sanyo, Japan). The medium needed to be refreshed after 3 days and the cell line was spliced after reaching 80 % confluence.

Cytotoxicity assay. HMEC-1 cells were seeded and left to grow to 80 % confluence at 37°C in a 5 % CO_2 incubator in a 96-well flat bottom plate. The NP samples were diluted to a defined concentration range (5, 10, 25, 50 µg/mL), starting from a stock solution of 197 µg/mL, in phenol red poor IMDM culture medium (MCDB 131 medium replaced by IMDM medium). Before adding 100 µL of each concentration to the cells, the latter were washed with 1xPBS (9 g/L NaCl, 0.795 g/L Na_2HPO_4, 0.144 g/L KH_2PO_4). A total of six wells per condition was taken and positive as well as negative control conditions were included. After an incubation period in the incubator of 24 h, the cells were washed 3 times with 1xPBS and a 10 % alamar blue solution in IMDM culture medium was added. After another 24 h, the resulting solution was transferred to an opaque-walled dark 96-well culture plate and the fluorescence was measured using a BMG Labtech FLUOstar OPTIMA (Temse, Belgium) at 590 nm with an excitation at 570 nm. The experiment was performed in triplicate. Data are represented as means ± standard deviation after analyzing with the commercially available software JMP Pro 12 (SAS Institute Inc., USA). Analysis of linear mixed model followed by a post-test Dunnett for multiple comparisons ($p < 0.05$) were performed.

Uptake Kinetics. HMEC-1 cells were seeded, employing a density of 100 000 cells per well, in a 24-well plate and left to grow for a 24 h period in a 5 % CO_2 atmosphere at 37 °C. First the cells were washed with 1xPBS after which 500 µL of 25 µg/mL of NPs in IMDM culture medium solution was added to the cells for a specific incubation period (5 min, 15 min, 30 min, 1 h, 2 h, 4 h, 6 h, 24 h and 30 h) at 37°C with a CO_2 level of 5%. After this period, the cells were washed 3 times with 1xPBS and harvested. Subsequently, the pellet was redispersed in 4 % PFA and left to incubate in the dark for 20 min at room temperature (RT). In order to remove the PFA, the cells were centrifuged 3 times after which the pellet was redispersed in fluorescence-activated cell sorting (FACS) buffer (1xPBS and 2 % FCS). The resulting samples were measured and analyzed with the Becton Dickinson LSR Fortessa (Erembodegem, Belgium). A 488 nm laser and 530/30 nm emission filter were employed and unlabeled cells were used as a blank to gate the signal. For each sample 20 000 cells were counted in triplicate. The number of cells that contained a fluorescent signal corresponding to NP uptake were

converted to a percent scale from 0 – 100 % with 100 % meaning that in all cells fluorescence was detected and thus NPs were present.

Confocal Laser Scanning Microscopy. HMEC-1 cells were left to adhere and grow for 24 h at 37 °C with a starting concentration of 20 000 cells per well in a µ-Slide 8-well plate (Ibidi). Subsequently, the cells were washed 3 times with 1xPBS after which 400 µL of 25 µg/mL of NPs in IMDM culture medium was added and left to incubate for a period of 24 h. The cells were washed 3 times with 1xPBS after which they were fixated with 4 % PFA for 20 min at RT in the dark. After this, the PFA solution was removed and the cells were washed an additional 3 times with 1xPBS. The images were collected at RT with a Zeiss (Zaventem, Belgium) LSM510 META NLO mounted on an inverted laser scanning microscope (Zeiss Axiovert 200 M) and a water immersion 40x/1.1 objective. Nanoparticle excitation was performed with an Argon-ion laser at 488 nm (3 µW maximum radiant power at the sample) and the emission was detected with a band-pass filter of 565-615 nm. The resulting 1024x1024 images were recorded using a pixel dwell time of 14.2 µs with a pixel size of 0.06 µm. The images were processed using ImageJ and AIM 4.2 software.

RESULTS & DISCUSSION

Synthesis of PPV-based NPs of different sizes

The particle formulation of PPV-based NPs of different sizes was performed using a combination of the miniemulsion technique and solvent evaporation approach. This process allows for a tunable NP diameter, surface functionality and solid content.[31, 32] Two types of preformed PPVs were employed, namely the homopolymer MDMO-PPV and statistical co-polymer CPM-*co*-MDMO-PPV (Figure S1). The latter is a polar functionalized PPV carrying an ester group on the alkoxy side chain that can be functionalized either by saponification or transesterification. The resulting NPs are expected to bear ester groups distributed on the surface and within the volume of the NPs, whereby the surface groups can be easily converted through hydrolysis into carboxylic acid groups. These chemical moieties are of particular interest as they can be employed for the straightforward incorporation of numerous

functional attributes. The negatively charged low molecular weight surfactant SDS was selected as the surfactant for the stabilization of the droplets (size tunable between 30 and 500 nm)[15].

To diminish the diameter of the PPV-based NPs, the polymer load used during preparation was scaled down while the amount of dispersed and continuous phases were kept constant.[33] The resulting characteristics of the red-colored water-based dispersion of PPV-based NPs (Figure S2) are summarized in table 1. Decreasing the amount of polymer from 50 mg to 5 mg led to a reduction in the hydrodynamic diameter from 51 nm to 17 nm for the CPM-*co*-MDMO-PPV NPs as shown by DLS as well as TEM (Figure S3-4). The size of the particles from the sample containing the lowest polymer concentration (1 mg) was difficult to determine from the TEM images owing to the irregular geometry and aggregation of the particles. The same effect was monitored for the MDMO-PPV NPs. However, it was observed that the polydispersity (PD) value of the nanoparticle formulations rose as the amount of polymer decreased. It has already been demonstrated that the employed synthesis method has the inherent characteristic of generating colloidal dispersion with a large size distribution.[32] In addition, for the same amount of the dispersed phase solvent, a larger amount of hydrophobic polymer within the emulsion droplets can also serve as an osmotic control agent, thereby leading to a narrowed size distribution for NPs of a bigger size.

Table 1. Formulation and Characteristics of the Synthesized PPV-based Nanoparticles (Mean ± SD)

Sample	Formulation	Polymer (mg)	Particle size DLS (nm)	Particle size TEM (nm)	Zeta potential (mV)
1a	CPM-*co*-MDMO-PPV	50	51 ± 13 PD = 0.102	53 ± 13	-42 ± 2
2a	CPM-*co*-MDMO-PPV	25	34 ± 10 PD = 0.132	31 ± 7	-31 ± 1
3a	CPM-*co*-MDMO-PPV	10	21 ± 8 PD = 0.204	30 ± 4	-23 ± 1

4a	CPM-*co*-MDMO-PPV	5	17 ± 6 PD = 0.226	22 ± 5	-23 ± 3
5a	CPM-*co*-MDMO-PPV	1	23 ± 4 PD = 0.350	-	-
1b	MDMO-PPV	50	51 ± 13 PD =0.108	54 ± 9	-40 ± 1
2b	MDMO-PPV	25	28 ± 10 PD =0.179	34 ± 7	-30 ± 1
3b	MDMO-PPV	10	23 ± 8 PD =0.174	27 ± 5	-28 ± 2
4b	MDMO-PPV	5	17 ± 7 PD =0.267	23 ± 3	-29 ± 1
5b	MDMO-PPV	1	20 ± 3 PD = 0.359	-	-

The zeta potential measurements indicate that with the decrease in size of the particles there is a drop in the magnitude of the values. Due to the very low solid content, the measurements with the samples containing the lowest polymer concentration did not yield consistent values. Given the excess of SDS that is extracted during the extensive washing steps, as demonstrated also by earlier research[20], the remaining NPs consist out of their respective PPV-derivative and the residual traces of SDS. However, in case of CPM-*co*-MDMO-PPV NPs, the presence of ester groups (susceptible to hydrolysis during the dispersion synthesis and washing steps) can influence the amount of SDS incorporated on the surface of the particles and the hydrolyzed ester groups can also contribute to the zeta potential values. As a consequence of synthesizing NPs through lowering the polymer content, it was required to reconcentrate the sample in order to be suitable to operate as a bioimaging probe without causing dilution induced effects. The resulting solid content was determined through UV-vis-

spectrophotometry rather than thermogravimetrically due to dilute samples (Figure S5). Following washing and reconcentrating, the solid content of the samples ranged from 1427 to 88 µg/mL for CPM-*co*-MDMO-PPV NPs and 907 to 197 µg/mL for MDMO-PPV NPs.

Influence of NP Size on Optical Characteristics of PPV-Based NPs

Subsequently, the influence of size reduction on the optical characteristics of the NPs was studied in detail employing different spectroscopic techniques. The absorbance and emission spectrum of the NPs in water (black lines) and molecularly dissolved polymer in chloroform (orange lines) were assessed using UV-vis and fluorescence spectroscopy for both the polymer types (Figure 1 and S6). Decreasing the NP size did not alter their characteristic broad adsorption band, ranging from 350 to 600 nm. The same implies for the emission spectrum, with regards to its characteristic vibronic structure (0-0, 0-1 and 0-2 emission bands at 590, 640 and 660 nm respectively), where no distinct difference was observed. This is in line with previous findings by Barbara et al., who showed that MEH-PPV based NPs are spectroscopically indistinguishable from each other and bulk thin films when their radius exceeds the size of 10 nm.[29] There is however a noticeable difference in the spectrum between the MDMO-PPV and CPM-*co*-MDMO-PPV NPs.
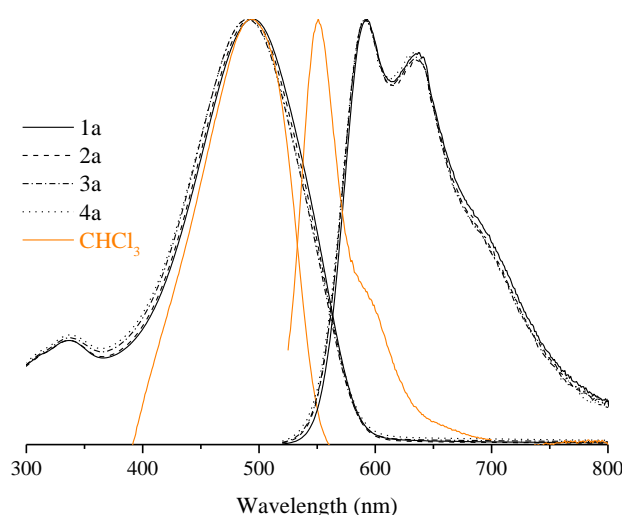

Figure 1. Absorbance (left) and emission (right) profile of CPM-*co*-MDMO-PPV NPs of various sizes (see table 1 and 2, black) as well as the molecularly dissolved polymer in chloroform (orange).

The shift in the emission maximum peak when going from molecularly dissolved chains (in chloroform) to NP (in water) configuration could be due to change from intrachain emission to

interchain emission when the conjugated polymers aggregate, during the evaporation of the solvent, into nanoparticles.[34] This is observed for both type of PPV nanoparticles as their emission shifts from 550 to 580 upon turning from molecularly dissolved chains (orange line Figure 1 and S6) into NP conformation (black line in Figure 1 and S6). The overlap of π-orbitals during aggregation can lead to red shift causing delocalization of the π-electrons across several chains leading to the formation of new electronic species with lower band gaps.[34, 35] However, a difference is noted in the relative height of the vibronic peaks between the two PPVs. For MDMO-PPV based NPs, a more substantial boost of the two low-energy red peaks occurs when compared to CPM-*co*-MDMO-PPV NPs. This observation can be correlated to the difference of the NPs' side chain, as that of CPM-*co*-MDMO-PPV is more polar. It is likely that this affects the chromophore packing during NP formation as well as the interactions of the exterior chains with the surrounding solvent. MDMO-PPV lacks these polar side chain groups and is therefore more prone to strong hydrophobic attraction between chains and large interfacial surface tension between the polymer and water. It encounters a larger drop in solvent quality as compared to CPM-*co*-MDMO-PPV, resulting in more kinking and bending of the polymer backbones and the subsequent stronger interchain interaction.[36] Therefore, CPM-*co*-MDMO-PPV NPs' main peak is the 0-0 band at 590 nm, while for MDMO-PPV NPs this shifts to the 0-1 band at 640 nm with an additional increase in the 0-2 band.[37, 38] The switch in the main peak location of small MDMO-PPV NPs can be attributed to the chain becoming more hydrophilic during the NP synthesis. It was shown that when working with small amounts of PPV, chemical defects might be more likely to occur during the synthesis.[39]

Several other inherent optical characteristics, besides the NP spectrum, are summarized in Table 2. Variation of NP size or polymer showed no distinct difference with regards to quantum yield as it retained its value of 1-2 %.[36] The molar extinction coefficient obtained at the λ_{max} lowered as the number of chromophores per NP decreases when the size becomes smaller, but remained in the order of 10^6 $M^{-1} \cdot cm^{-1}$.[36] The size variation did not have a detrimental effect on the fluorescence brightness, the product of the quantum yield and the molar extinction coefficient, which is one of the determining factors for a successful imaging probe.

Table 2. Optical Characteristics of the Synthesized PPV-based Nanoparticles

Sample	λ_{max} excitation (nm)	λ_{max} emission (nm)	Quantum Yield (φ_F, %)	Molar extinction coefficient (ε, M$^{-1}\cdot$ cm^{-1})	Absorption cross section (σ, cm²)
1a	494	593	2	13.1×10^6	5.00×10^{-14}
2a	493	591	2	10.2×10^6	3.91×10^{-14}
3a	490	591	2	$9,9 \times 10^6$	3.80×10^{-14}
4a	490	592	1	9.7×10^6	3.71×10^{-14}
1b	494	636	2	11.7×10^6	4.47×10^{-14}
2b	494	638	1	9.5×10^6	3.65×10^{-14}
3b	492	636	1	9.5×10^6	3.62×10^{-14}
4b	495	592	1	6.4×10^6	2.46×10^{-14}

In order to investigate the limit of lowering the amount of PPV to synthesize smaller NPs with the employed synthesis method, an additional sample was made using only 1 mg of the respective polymers (Figure 2 and S7). For both systems, a transformation in the colloidal dispersion color from red to orange (MDMO-PPV) and yellow (CPM-*co*-MDMO-PPV) was observed. In addition, the CPM-*co*-MDMO-PPV NPs absorbance intensity lowered and both NP systems demonstrated a blue

shift in the excitation as well as emission spectrum. This latter feature signifies a shortening in the average conjugation length of the conjugated polymer.[37]
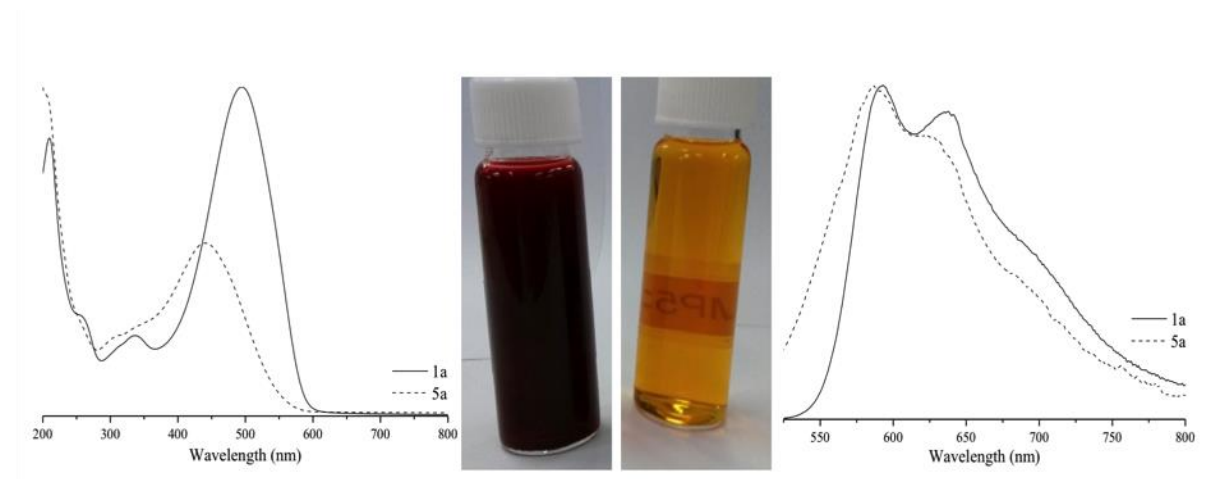
Figure 2. Absorbance (left) and emission (right) profile of CPM-*co*-MDMO-PPV NPs with low starting polymer concentration (right vial, 1 mg, 5a) as compared to a high one (left vial, 50 mg, 1a).

In order to determine if the conjugation length shortening was a temporary or permanent characteristic CPM-*co*-MDMO-PPV NPs were redissolved in CHCl$_3$ and the spectra of the free molecular chains measured (Figure 3). If the blue shift was caused by a reversible effect, such as torsion of the polymer backbone, no difference should be observed between the spectra of both samples. Sample 1a exhibited the innate behavior of the system when dissolved in CHCl$_3$, namely an alteration in the emission maximum to 550 nm and a narrowing of the absorbance spectrum nm due to the disappearance of aggregates.[20] However, sample 5a displayed a blue shift in absorbance maximum to 417 nm, loss of the vibronic structure and the appearance of a blue shoulder in the emission spectrum. This clearly demonstrates that the change in conjugation length is a permanent feature.
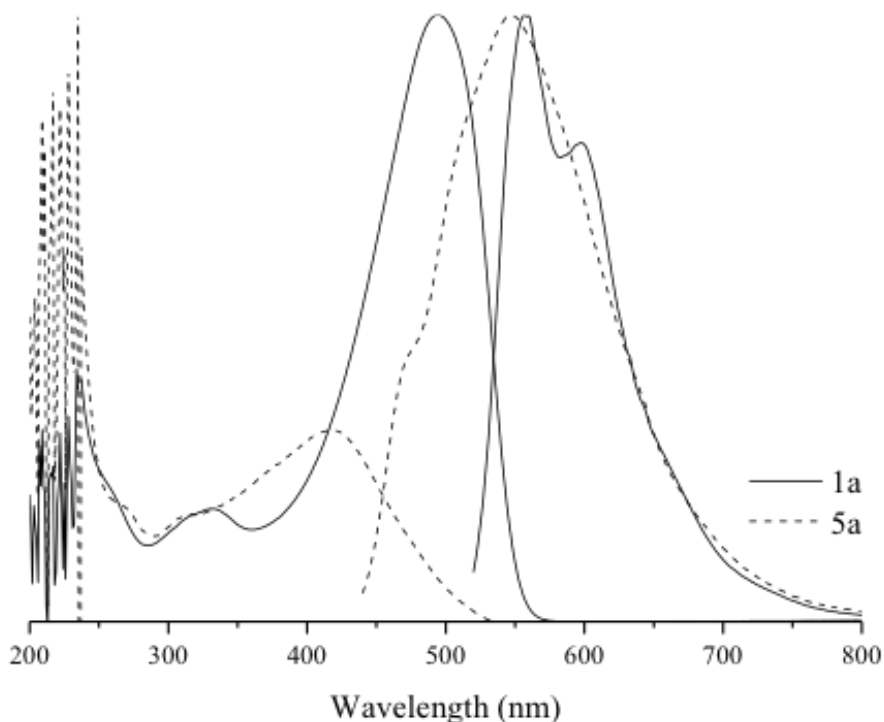
Figure 3. Spectrum of molecular chains of redissolved CPM-*co*-MDMO-PPV NPs in CHCl$_3$ of low

(1a) and high (5a) starting polymer concentration.

It is well documented that exocyclic double bonds in PPVs are prone to photo-oxidation, a process which potentially can disrupt the π-conjugation.[40] Because the 5a NPs consist of only a few polymer chains as compared to variants 1a – 4a, resulting in a higher surface-to-volume ratio, it is probable that the chains in the configuration are more exposed to photoinduced oxidation, chain scission and opening of the conjugated system, as these processes are much more severe at the surface where solar irradiation takes place.[39, 41] The difference between CPM-*co*-MDMO-PPV NPs and MDMO-PPV NPs can be attributed to the hydrophilic side chains of the former. Swelling behavior at the interface might induce extra void space between the chain coils, allowing for oxygen to diffuse more readily to the photoexcited regions and resulting in an increase of the rate at which damage occurs.[37] In addition, chain degradation can also occur due to exposure to ultrasonication.[35]

Influence of NP size on Biological Characteristics of PPV-Based NPs

As it has been established that the size of nanoparticles plays an important role in the interaction with their biological surroundings, the influence of size modification on the biological characteristics was studied. Although it was shown earlier that CPM-*co*-MDMO-PPV and MDMO-PPV based NPs of 100 nm size are not cytotoxic[20], reducing the diameter can have a detrimental effect on the biocompatibility.[42-44] Therefore, it is of importance to re-evaluate the cytotoxicity of PPV-based NPs of various sizes. Cytotoxicity experiments were conducted on HMEC-1 cells as endothelial cells make up the blood vessels and are therefore one of the first cell-types that NPs will encounter upon being administered.

The alamar blue assay results showed that size did influence the biocompatibility of PPV-based NPs (Figure 4 and S8). For the higher concentrations there was a slight statistically significant reduction on viability independent of size. However, cell viability never dropped below 90 % after an exposure period of 24 h, which is in agreement with previous results.[20] Accordingly, it can be concluded that varying the size of PPV-based NPs does not have a negative impact on cell viability. Sample 4a was excluded from the cytotoxicity and uptake studies, given the concentration was too low to conduct the biomedical experiments with.
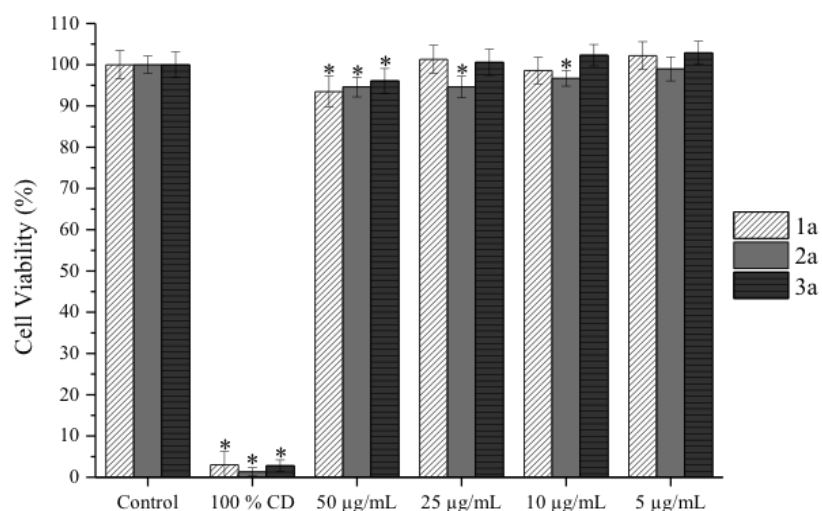
Figure 4. Dose-dependent cytotoxicity of CPM-*co*-MDMO-PPV NPs of different sizes after 24 h of exposure determined by the alamar blue assay in HMEC-1 cells. CD = cell death. Data are expressed as percent of control mean ± SD (N = 3).

In addition to this, the uptake by cells as a function of time for the different NP sizes was monitored using flow cytometry (Figure 5) and confocal microscopy (Figure S9 and S10). A clear difference is visible in the uptake profiles of NPs of different sizes. For MDMO-PPV NPs, decreasing the size led to a clear increase in the rate of uptake, while for CPM-*co*-MDMO-PPV NPs this effect was less pronounced. After 30h of incubation with a concentration of 25 µg/mL the amount of cells that have taken up NPs is almost double for MDMO-PPV NPs when comparing the smallest and biggest constructed NPs. This difference between the NP configurations can be attributed to the already fast uptake of CPM-*co*-MDMO-PPV NPs due to an increased negative surface charge.[20] As stated earlier we previously showed[20] that after washing a zeta potential difference is observable between CPM-*co*-MDMO-PPV NPs and MDMO-PPV NPs due to hydrolysis of ester group, which increases uptake.
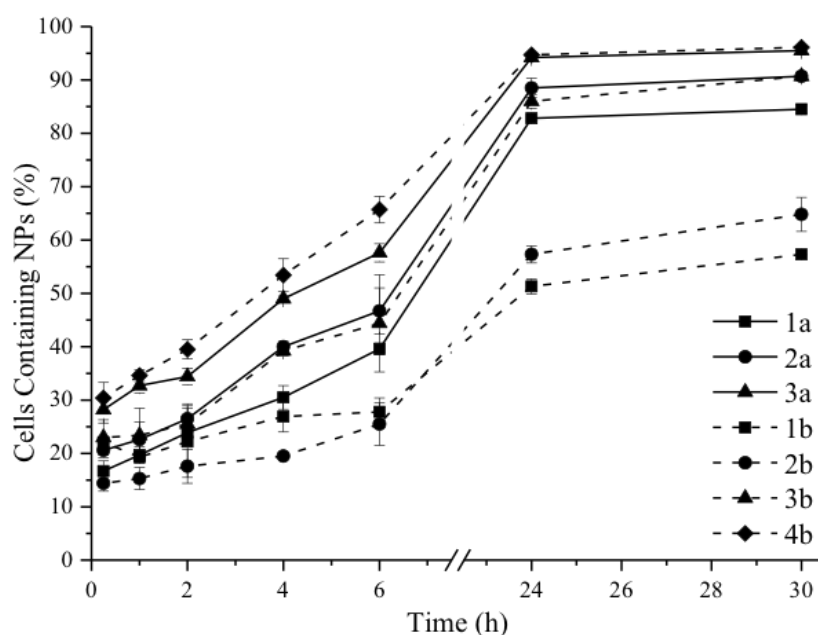
Figure 5. Kinetics of uptake: Internalization of CPM-*co*-MDMO-PPV (solid line) and MDMO-PPV (dashed line) NP of different sizes by HMEC-1 cells over a time period of 30 h.

A size related pattern in the amount of uptake was also observed visually using confocal laser scanning microscopy. The fluorescent NPs remained stable in cell culture medium and were indeed taken up by the HMEC-1 cells within the set incubation period, without causing any negative effects on the integrity of cell morphology. A boost in uptake for both NP systems was visible when the size of the NPs was lowered. This feature allows for the construction of a system that can be easily modified to have the right size and functionality to achieve a set biomedical target.

CONCLUSION

MDMO-PPV and CPM-*co*-MDMO-PPV NPs of various sizes were successfully synthesized through the combination of the miniemulsion and solvent-evaporation method by lowering the amount of polymer systematically in the formulation. By changing the amount of polymer used during the synthesis from 50 to 5 mg, the size of the NPs could be decreased from 50 to 17 nm for both configurations. However, the combination of employing the miniemulsion and solvent evaporation technique and lowering the hydrophobic polymer content has the inherent drawback of increasing the polydispersity index of the colloidal solution. An investigation of the optical properties revealed that size did not have an influence on the optical properties of the PPV-base NP configurations within the tested range. The photoluminescence spectrum of both MDMO-PPV and CPM-*co*-MDMO-PPV NPs showed the characteristic vibronic structure with 0-0, 0-1 and 0-2 emission bands at 590, 640 and 660 nm. A difference between the two PPV models was observed, namely MDMO-PPV having its main peak shifted from 590 to 640 nm, which can be attributed to the lack of a hydrophilic group in its side-chain. No substantial changes were observed in the fluorescent brightness of the NPs, determined by the quantum yield and molar extinction coefficient, as well. However, for very small NPs constructed by lowering the amount of polymer below 5 mg, a permanent change in the conjugation length was observed. This observed phenomenon could be attributed to photoinduced oxidation, a well-known hurdle of PPVs. Cell studies demonstrated that decreasing the size of the NPs does not lower the cell viability below 90 % but does influence the rate and amount of uptake. An effect that is even more pronounced for the MDMO-PPV variant, which is taken up more slowly due to the lack of an additional surface charge compared to CPM-*co*-MDMO-PPV. The results presented highlight that PPV-based NPs are an excellent candidate for bioimaging applications owing to their high design flexibility, which does not show adverse effects on their interesting optical properties or benign biological characteristics.

AUTHOR INFORMATION

Corresponding Author

* E-mail: anitha.ethirajan@uhasselt.be

Phone number: +32-11268877

Notes

The authors declare no competing financial interest.

Author Contributions

The manuscript was written through contributions of all authors. All authors have given approval to the final version of the manuscript.

References:

1.   Kubitscheck U. Fluorescence microscopy: from principles to biological applications: John Wiley & Sons; 2017.
2.   Lichtman JW, Conchello J-A. Fluorescence microscopy. Nature methods. 2005;2(12):910.
3.   Pepperkok R, Ellenberg J. High-throughput fluorescence microscopy for systems biology. Nat Rev Mol Cell Biol. 2006;7(9):690-6.
4.   Advanced Fluorescence Reporters in Chemistry and Biology III: Applications in Sensing and Imaging: Springer; 2011.
5.   Jaiswal JK, Simon SM. Potentials and pitfalls of fluorescent quantum dots for biological imaging. Trends in cell biology. 2004;14(9):497-504.
6.   Michalet X, Pinaud FF, Bentolila LA, Tsay JM, Doose S, Li JJ, et al. Quantum Dots for Live Cells, in Vivo Imaging, and Diagnostics. Science. 2005;307(5709):538-44.
7.   Resch-Genger U, Grabolle M, Cavaliere-Jaricot S, Nitschke R, Nann T. Quantum dots versus organic dyes as fluorescent labels. Nat Meth. 2008;5(9):763-75.
8.   Alford R, Simpson HM, Duberman J, Hill GC, Ogawa M, Regino C, et al. Toxicity of organic fluorophores used in molecular imaging: literature review. Molecular imaging. 2009;8(6):7290.2009. 00031.
9.   Bradburne CE, Delehanty JB, Boeneman Gemmill K, Mei BC, Mattoussi H, Susumu K, et al. Cytotoxicity of Quantum Dots Used for In Vitro Cellular Labeling: Role of QD Surface Ligand, Delivery Modality, Cell Type, and Direct Comparison to Organic Fluorophores. Bioconjugate Chem. 2013;24(9):1570-83.
10.   Hofmann D, Messerschmidt C, Bannwarth MB, Landfester K, Mailander V. Drug delivery without nanoparticle uptake: delivery by a kiss-and-run mechanism on the cell membrane. Chem Commun. 2014;50(11):1369-71.
11.   Penjweini R, Deville S, D'olieslaeger L, Berden M, Ameloot M, Ethirajan A. Intracellular localization and dynamics of Hypericin loaded PLLA nanocarriers by image correlation spectroscopy. Journal of Controlled Release. 2015;218:82-93.
12.   Reisch A, Klymchenko AS. Fluorescent Polymer Nanoparticles Based on Dyes: Seeking Brighter Tools for Bioimaging. Small. 2016;12(15):1968-92.
13.   Mochalin VN, Shenderova O, Ho D, Gogotsi Y. The properties and applications of nanodiamonds. Nature nanotechnology. 2012;7(1):11.
14.   Heeger AJ. Semiconducting polymers: the Third Generation. Chemical Society Reviews. 2010;39(7):2354-71.
15.   Tuncel D, Demir HV. Conjugated polymer nanoparticles. Nanoscale. 2010;2(4):484-94.
16.   Wu C, Chiu DT. Highly Fluorescent Semiconducting Polymer Dots for Biology and Medicine. Angewandte Chemie International Edition. 2013;52(11):3086-109.
17.   Yu J, Rong Y, Kuo C-T, Zhou X-H, Chiu DT. Recent advances in the development of highly luminescent semiconducting polymer dots and nanoparticles for biological imaging and medicine. Analytical chemistry. 2016;89(1):42-56.
18.   Zaquen N, Lu H, Chang T, Mamdooh R, Lutsen L, Vanderzande D, et al. Profluorescent PPV-Based Micellar System as a Versatile Probe for Bioimaging and Drug Delivery. Biomacromolecules. 2016;17(12):4086-94.
19.   Ethirajan A, D'Olieslaeger L, Vandenbergh J, Lutsen L, D'Olieslaeger M, Vanderzande D, et al. Synthesis of MDMO-PPV Nanoparticles Via In Situ Sulfinyl Precursor Route Polymerization in Miniemulsion. Macromolecular Chemistry and Physics. 2013;214(16):1859-64.
20.   Peters M, Zaquen N, D'Olieslaeger L, Bové H, Vanderzande D, Hellings N, et al. PPV-Based Conjugated Polymer Nanoparticles as a Versatile Bioimaging Probe: A Closer Look at the Inherent Optical Properties and Nanoparticle–Cell Interactions. Biomacromolecules. 2016.
21.   D'Olieslaeger L, Braeken Y, Cheruku S, Smits J, Ameloot M, Vanderzande D, et al. Tuning the optical properties of poly (p-phenylene ethynylene) nanoparticles as bio-imaging probes by side chain functionalization. Journal of Colloid and Interface Science. 2017.

22.   van Breemen AJJM, Vanderzande DJM, Adriaensens PJ, Gelan JMJV. Highly Selective Route for Producing Unsymmetrically Substituted Monomers toward Synthesis of Conjugated Polymers Derived from Poly(p-phenylene vinylene). The Journal of Organic Chemistry. 1999;64(9):3106-12.

23.   Vandenbergh J, Cosemans I, Lutsen L, Vanderzande D, Junkers T. Controlled synthesis of MDMO-PPV and block copolymers made thereof. Polymer Chemistry. 2012;3(7):1722-5.

24.   Junkers T, Vandenbergh J, Adriaensens P, Lutsen L, Vanderzande D. Synthesis of poly(p-phenylene vinylene) materials via the precursor routes. Polymer Chemistry. 2012;3(2):275-85.

25.   Zaquen N, Vandenbergh J, Schneider-Baumann M, Lutsen L, Vanderzande D, Junkers T. Facile Synthesis of Well-Defined MDMO-PPV Containing (Tri) Block—Copolymers via Controlled Radical Polymerization and CuAAC Conjugation. Polymers. 2015;7(3):418-52.

26.   Duchateau J, Lutsen L, Guedens W, Cleij TJ, Vanderzande D. Versatile post-polymerization functionalization of poly(p-phenylene vinylene) copolymers containing carboxylic acid substituents: development of a universal method towards functional conjugated copolymers. Polymer Chemistry. 2010;1(8):1313-22.

27.   Salatin S, Maleki Dizaj S, Yari Khosroushahi A. Effect of the surface modification, size, and shape on cellular uptake of nanoparticles. Cell biology international. 2015;39(8):881-90.

28.   Shang L, Nienhaus K, Nienhaus GU. Engineered nanoparticles interacting with cells: size matters. Journal of nanobiotechnology. 2014;12(1):5.

29.   Grey JK, Kim DY, Norris BC, Miller WL, Barbara PF. Size-Dependent Spectroscopic Properties of Conjugated Polymer Nanoparticles. J Phys Chem B. 2006;110(51):25568-72.

30.   D'Olieslaeger L, Pirotte G, Cardinaletti I, D'Haen J, Manca J, Vanderzande D, et al. Eco-friendly fabrication of PBDTTPD: PC 71 BM solar cells reaching a PCE of 3.8% using water-based nanoparticle dispersions. Organic Electronics. 2017;42:42-6.

31.   Landfester K. The generation of nanoparticles in miniemulsions. Advanced Materials. 2001;13(10):765-8.

32.   Staff RH, Schaeffel D, Turshatov A, Donadio D, Butt HJ, Landfester K, et al. Particle Formation in the Emulsion-Solvent Evaporation Process. Small. 2013;9(20):3514-22.

33.   Musyanovych A, Schmitz-Wienke J, Mailänder V, Walther P, Landfester K. Preparation of biodegradable polymer nanoparticles by miniemulsion technique and their cell interactions. Macromolecular bioscience. 2008;8(2):127-39.

34.   Schwartz BJ. CONJUGATED POLYMERS AS MOLECULAR MATERIALS: How Chain Conformation and Film Morphology Influence Energy Transfer and Interchain Interactions. Annual Review of Physical Chemistry. 2003;54(1):141-72.

35.   Howes P, Green M, Levitt J, Suhling K, Hughes M. Phospholipid Encapsulated Semiconducting Polymer Nanoparticles: Their Use in Cell Imaging and Protein Attachment. Journal of the American Chemical Society. 2010;132(11):3989-96.

36.   Sun K, Chen H, Wang L, Yin S, Wang H, Xu G, et al. Size-dependent property and cell labeling of semiconducting polymer dots. ACS applied materials & interfaces. 2014;6(13):10802-12.

37.   Nguyen T-Q, Martini IB, Liu J, Schwartz BJ. Controlling Interchain Interactions in Conjugated Polymers: The Effects of Chain Morphology on Exciton−Exciton Annihilation and Aggregation in MEH−PPV Films. The Journal of Physical Chemistry B. 2000;104(2):237-55.

38.   Groff LC, Jiang Y, Wang X, McNeill JD. Effect of Swelling on Multiple Energy Transfer in Conjugated Polymer Nanoparticles. The Journal of Physical Chemistry C. 2017;121(13):7549-57.

39.   Clafton SN, Beattie DA, Mierczynska-Vasilev A, Acres RG, Morgan AC, Kee TW. Chemical defects in the highly fluorescent conjugated polymer dots. Langmuir. 2010;26(23):17785-9.

40.   Manceau M, Bundgaard E, Carlé JE, Hagemann O, Helgesen M, Søndergaard R, et al. Photochemical stability of π-conjugated polymers for polymer solar cells: a rule of thumb. Journal of Materials Chemistry. 2011;21(12):4132-41.

41.   Yan M, Rothberg LJ, Papadimitrakopoulos F, Galvin ME, Miller TM. Defect Quenching of Conjugated Polymer Luminescence. Physical Review Letters. 1994;73(5):744-7.

42.   Park MVDZ, Neigh AM, Vermeulen JP, de la Fonteyne LJJ, Verharen HW, Briedé JJ, et al. The effect of particle size on the cytotoxicity, inflammation, developmental toxicity and genotoxicity of silver nanoparticles. Biomaterials. 2011;32(36):9810-7.

43.   Pan Y, Neuss S, Leifert A, Fischler M, Wen F, Simon U, et al. Size-Dependent Cytotoxicity of Gold Nanoparticles. Small. 2007;3(11):1941-9.

44.   Napierska D, Thomassen LCJ, Rabolli V, Lison D, Gonzalez L, Kirsch-Volders M, et al. Size-Dependent Cytotoxicity of Monodisperse Silica Nanoparticles in Human Endothelial Cells. Small. 2009;5(7):846-53.

Size-Dependent Properties of Functional PPV-based Conjugated Polymer Nanoparticles for Bioimaging.

Martijn Peters[a], Senne Seneca[a], Niels Hellings[c], Tanja Junkers[a,b], Anitha Ethirajan[a,b]*.

[a] Institute for Materials Research, Hasselt University, Martelarenlaan 42, 3500 Hasselt, Belgium.

[b] Imec associated lab IMOMEC, Wetenschapspark 1, 3590 Diepenbeek, Belgium.

[c] Immunology-Biochemistry, Biomedical Research Institute, Hasselt University, Agoralaan Building C, 3590 Diepenbeek, Belgium.

Corresponding Author Details:

E-mail: anitha.ethirajan@uhasselt.be

Phone number: +32-11268877

SUPPLEMENTARY INFORMATION

RESULTS
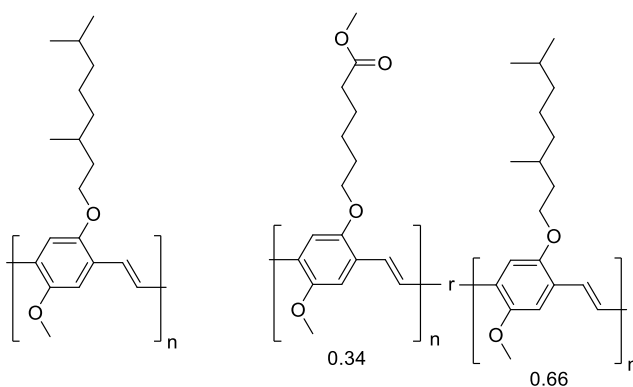
Figure S1. Chemical structure of the used PPV-derivatives: MDMO-PPV (*left*) and CPM-PPV-co-MDMO-PPV (34:66 copolymer ratio) (right).
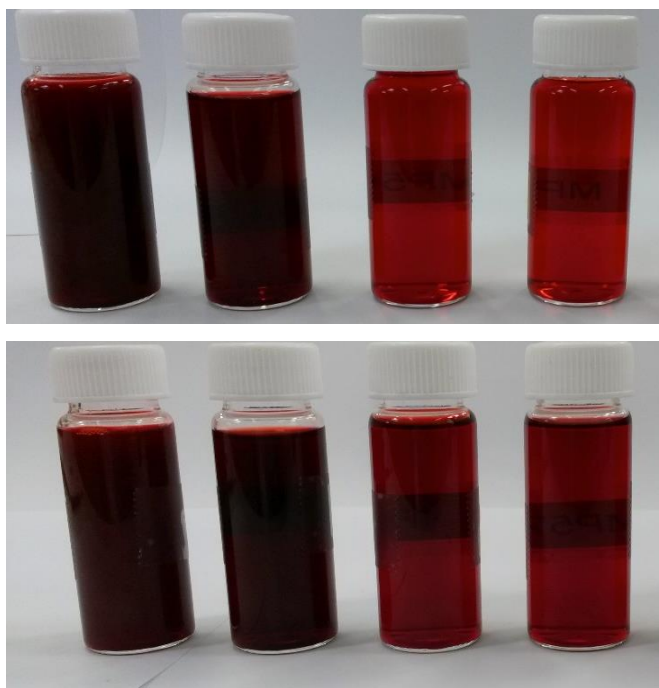
Figure S2. CPM-*co*-MDMO-PPV (top) and MDMO-PPV NPs (bottom) with different amounts of conjugated polymer (left to right: 50, 25, 10 and 5 mg) in a water-based dispersion formulation.
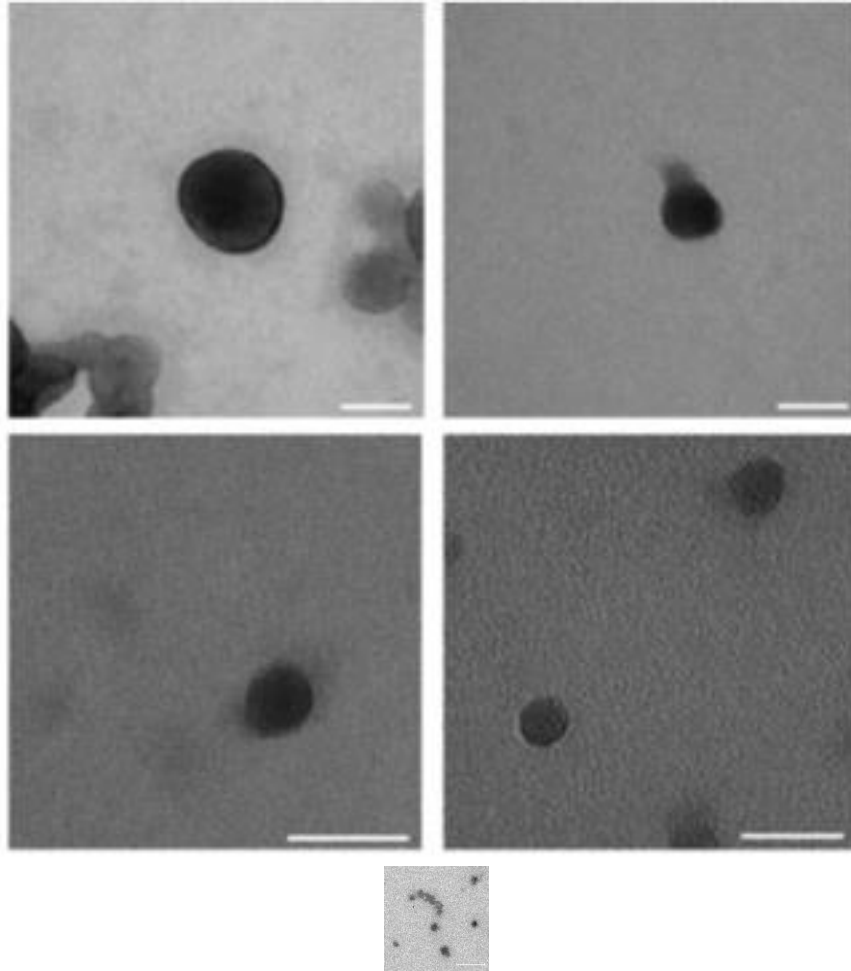
Figure S3. TEM image of CPM-*co*-MDMO-PPV NPs with different sizes (top left – 1a, top right – 2a, middle left – 3a, middle right – 4a, bottom– 5a). Scale bar represents 50 nm, except for sample 5a where the scale bar corresponds to 500 nm.
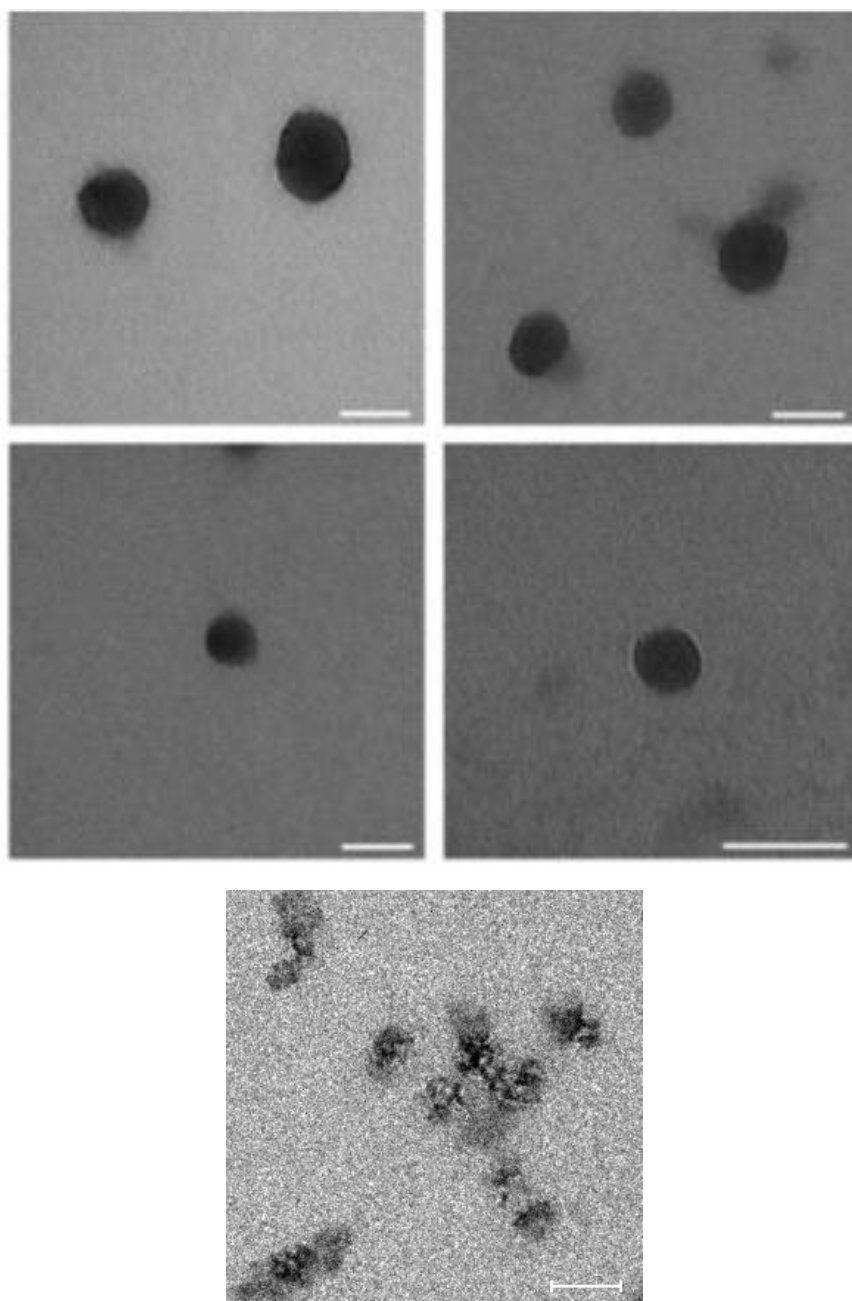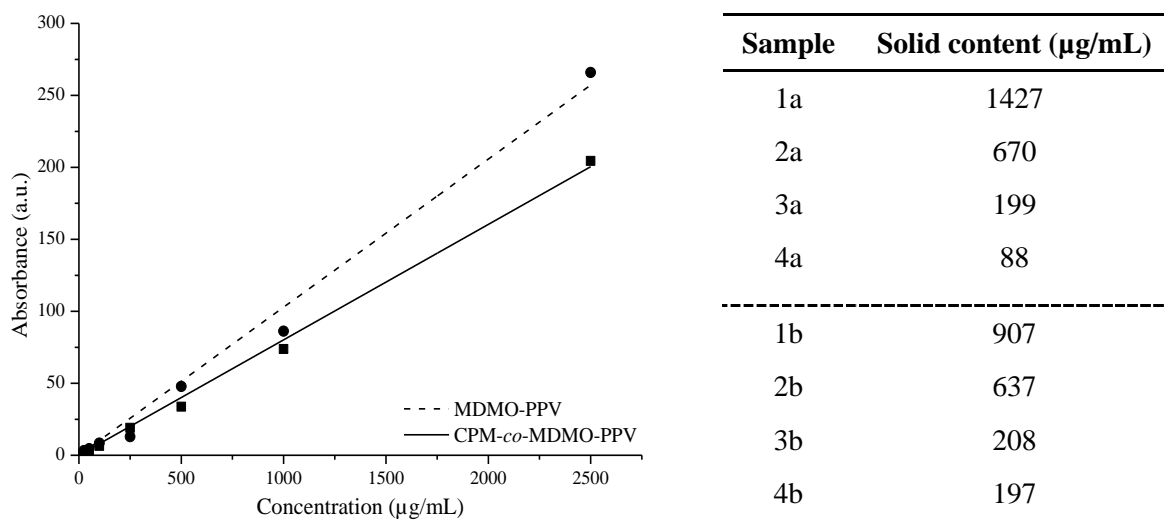
Figure S4. TEM image of MDMO-PPV NPs with different sizes (top left – 1b, top right – 2b, middle left – 3b, middle right – 4b, bottom– 5b). Scale bar represents 50 nm, except for sample 5b where the scale bar corresponds to 100 nm.

Sample	Solid content (µg/mL)
1a	1427
2a	670
3a	199
4a	88
1b	907
2b	637
3b	208
4b	197

Figure S5. UV-spectrophotometric determination of NP solid content
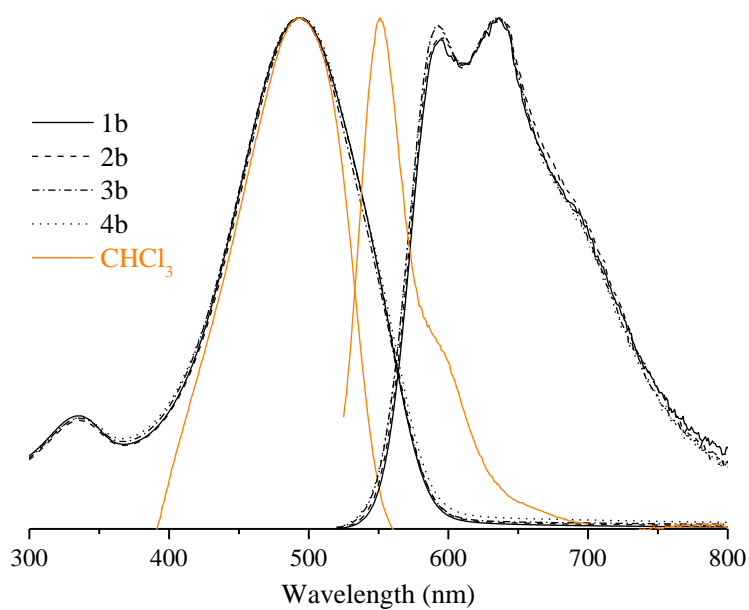
Figure S6. Absorbance (left) and emission (right) profile of MDMO-PPV NPs of various sizes (black) as well as the molecularly dissolved polymer in chloroform (orange).
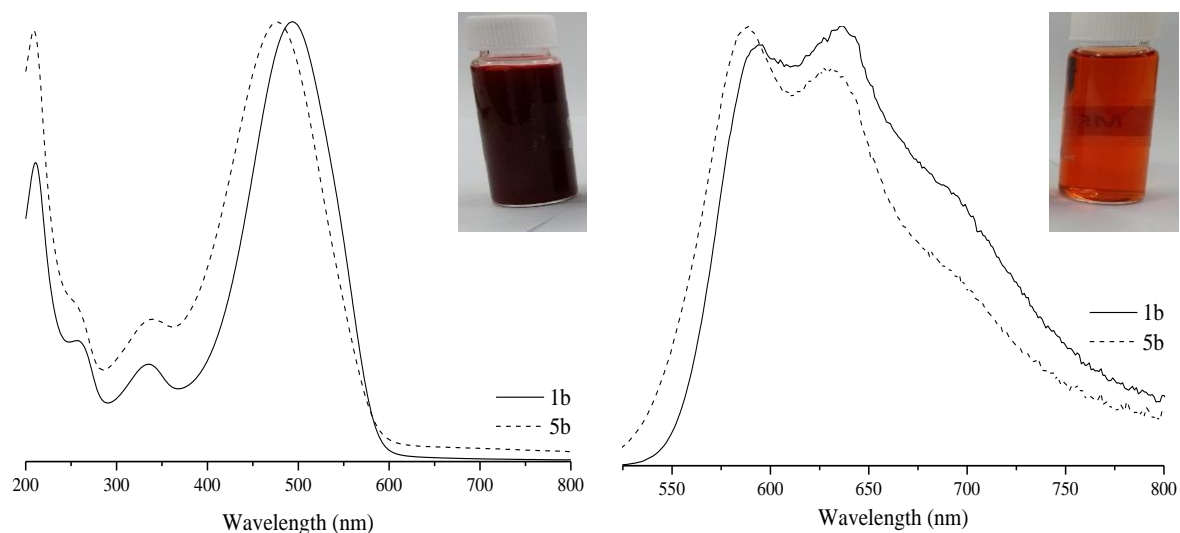
Figure S7. Absorbance (left) and emission (right) profile of MDMO-PPV NPs with low starting polymer concentration (right vial, 1 mg, 5b) as compared to a high one (left vial, 50 mg, 1b).
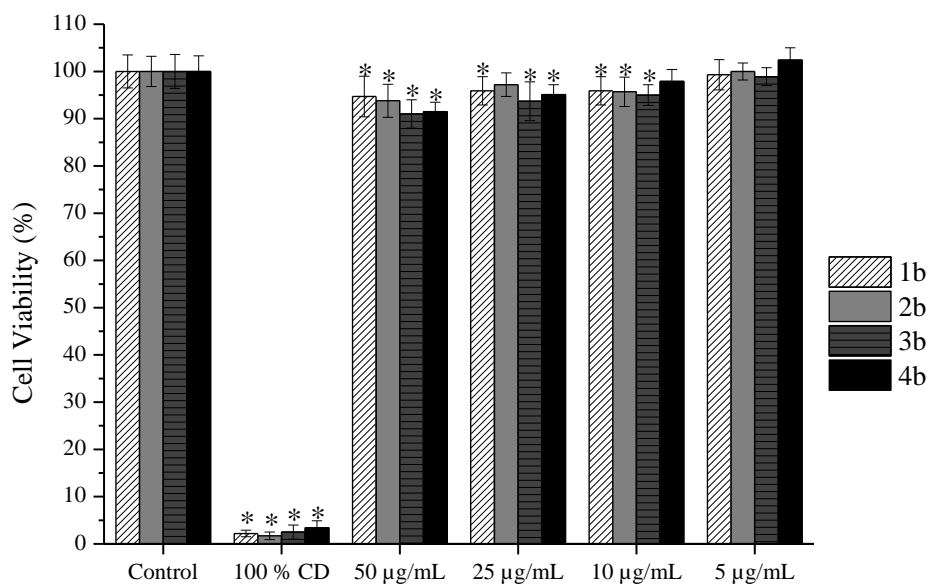

Figure S8. Dose-dependent cytotoxicity of MDMO-PPV NPs of different sizes after 24 h of exposure determined by the alamar blue assay in HMEC-1 cells. CD = cell death. Data are expressed as percent of control mean ± SD (N = 3).
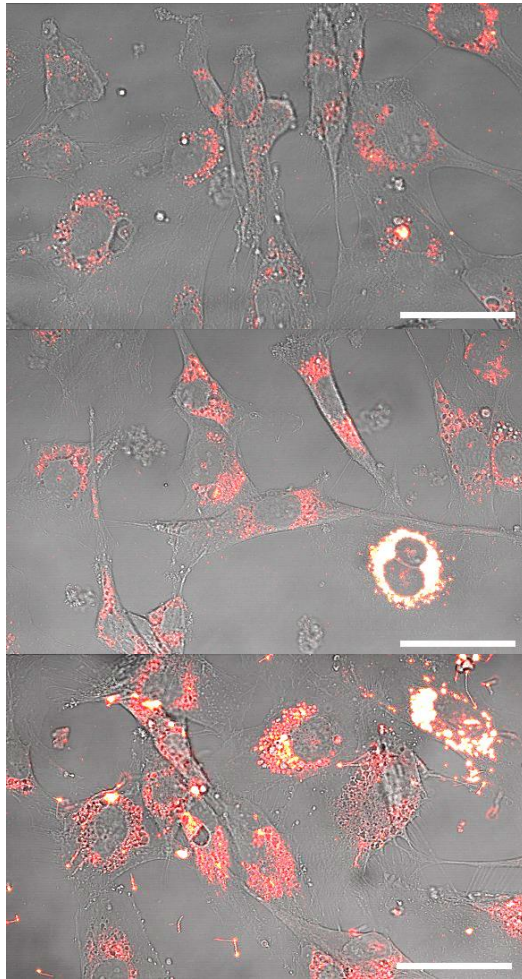
Figure S9. Confocal microscope image of HMEC-1 cells treated with CPM-*co*-MDMO-PPV NPs of different sizes (1a – top, 2a – middle, 3a – bottom) for an incubation period of 24 h. Scale bar represents 50 μm.
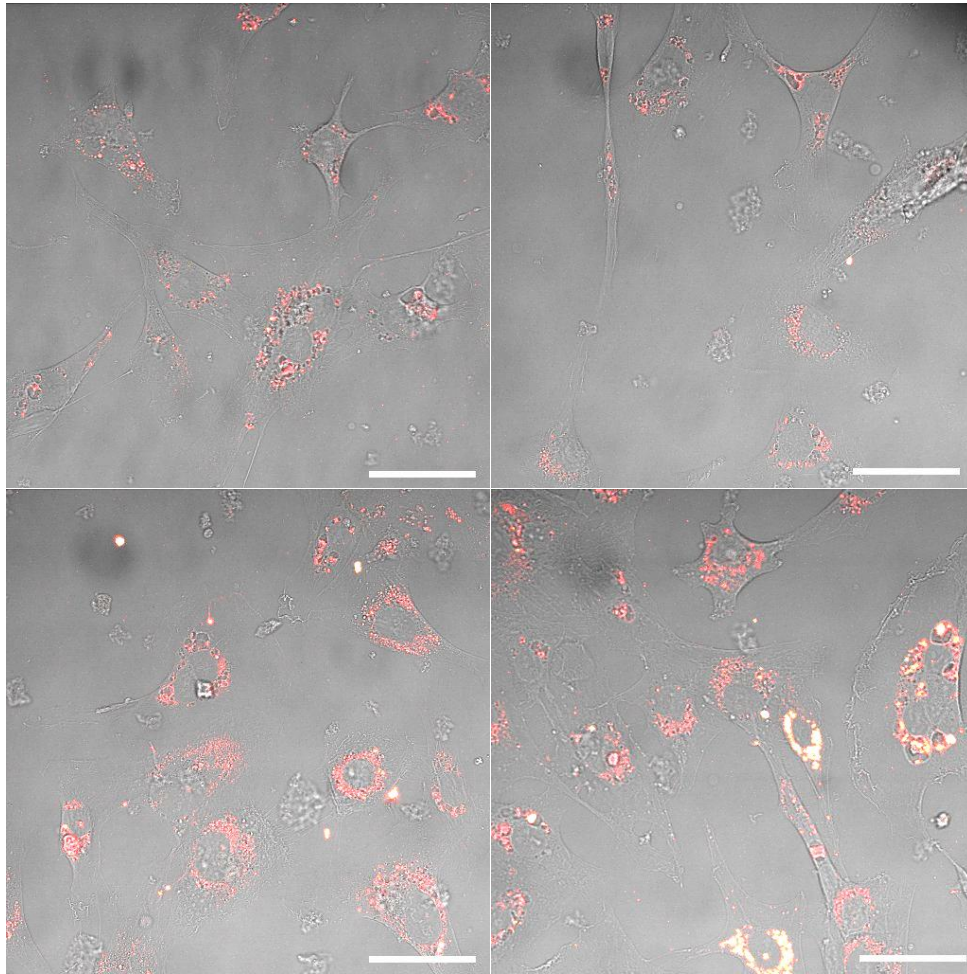
Figure S10. Confocal microscope image of HMEC-1 cells treated with MDMO-PPV NPs of different sizes (1b – top left, 2b – top right, 3b – bottom left, 4b – bottom right) for an incubation period of 24 h. Scale bar represents 50 μm.